

Phosphorus-rich biochar produced through bean-worm skin waste pyrolysis enhances the adsorption of aqueous lead

Yubo Yan^{a,b}, Binoy Sarkar^c, Lei Zhou^a, Ling Zhang^d, Qiao Li^e, Jianjun Yang^{b*}, Nanthi Bolan^{f,g}

^a*School of Chemistry and Chemical Engineering, Huaiyin Normal University, Huai'an 223300, China*

^b*Institute of Environmental and Sustainable Development in Agriculture, Chinese Academy of Agricultural Science, Beijing 100081, China*

^c*Lancaster Environment Centre, Lancaster University, Lancaster, LA1 4YQ, United Kingdom*

^d*School of Health, Jiangsu Food & Pharmaceutical Science College, Huai'an 223001, China*

^e*School of Environmental and Biological Engineering, Nanjing University of Science and Technology, Nanjing 210094, China*

^f*Global Centre for Environmental Remediation, University of Newcastle, Callaghan Campus, NSW 2308, Australia*

^g*Cooperative Research Centre for High Performance Soil (Soil CRC), Callaghan, NSW 2308, Australia*

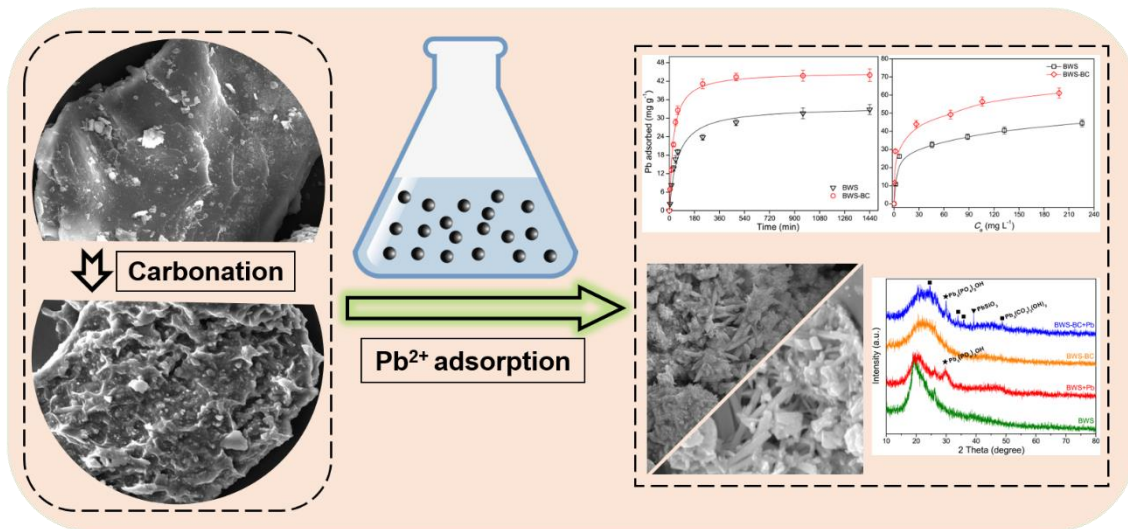
Corresponding author:

Prof Jianjun Yang (yangjianjun@caas.cn)

Highlights

- > A novel phosphorus (P) rich biochar (BWS-BC) was produced from bean-worm skin waste.
- > BWS-BC was effective in adsorption of Pb(II) from wastewater.
- > BWS-BC showed a fast initial adsorption rate in Pb(II) adsorption.
- > P in BWS-BC played an important role in Pb(II) adsorption.

Graphical abstract



Abstract: In China, more than 10,000 tons of bean-worm powder, which is rich in protein (68.5%) and essential amino acids (52.8%), is consumed annually. Thus, a large amount of bean-worm skin waste is generated, and is often indiscriminately disposed of, potentially causing environment problems. In this study, bean-worm skin waste (BWS) was pyrolyzed at 500°C to produce biochar (BWS-BC), and the surface properties of BWS-BC were characterized using advanced spectroscopic techniques. Pb(II) adsorption properties of BWS and the corresponding biochar as a function of solution pH, contact time, and equilibrium concentration of Pb(II) were examined using adsorption isotherm, kinetics, thermodynamic studies, and spectroscopic techniques. The maximum Pb(II) adsorption capacities based on the Langmuir isotherm model were calculated as 45 and 62 mg g⁻¹ for BWS and BWS-BC, respectively, which were comparable to the values obtained for biochars derived from other agro-wastes. The adsorption feasibility, favorability and spontaneity of Pb(II), as derived from the thermodynamic parameters, indicated that chemisorption and precipitation (e.g., hydroxypyromorphite) were the main adsorption mechanism in case of BWS and BWS-BC, respectively. Thus, conversion of BWS to biochar for Pb(II) adsorption can be considered as a feasible, promising and high value-added approach for BWS recycling.

Keywords: Pb(II) removal, Waste bean worm skin, Biochar, Adsorption mechanism, Wastewater treatment

1. Introduction

Recycling of agricultural wastes as adsorbents for wastewater treatment has received much attention since these wastes are of low-cost, readily available and eco-friendly (Anastopoulos et al., 2019; Lingamdinne et al., 2016). For example, Fernández-López et al. (2019) showed that agro-waste from globe artichoke was effective in adsorbing aqueous Pb(II), Cu(II) and Cd(II). Wierzba and Kłós (2019) demonstrated the possibility of utilization of brewer's spent grain for the adsorption of aqueous heavy metals, and its adsorption effectiveness was related to the presence of other cations in the wastewater. Semerjian (2018) found that adsorption of heavy metals by natural pine sawdust (*Pinus halepensis*) was spontaneous and endothermic, and the adsorption capacity of Pb(II) and Cu(II) was 13.48 and 9.59 mg g⁻¹, respectively. Gorgievski et al. (2013) reported that wheat straw could be a potential adsorbent to remove heavy metals from weakly acidic effluents, and its adsorption capacity ranged from 2.49 to 4.9 mg g⁻¹. Vilardi et al. (2018) used banana peel powder to adsorb heavy metals, and its maximum adsorption capacity of Pb(II) and Cu(II) was 10.9 and 12.85 mg g⁻¹, respectively. There are still a lot of similar studies such as the utilization of watermelon rind, potato peel, cucumber peel and peanut shell as adsorbents (Anastopoulos et al., 2019). A general survey of relevant literature showed that (i) recent research interests in this topic were principally focused on the plant-based wastes, but little on insect-based wastes, and (ii) majority of biomass adsorbents were often restricted from practical applications due to the low adsorption capacity and poor stability of the adsorbents.

Shortage of food resources (especially for animal protein), as a result of the growth of world population and further degradation of the environment, has impacted the human societies for

decades. Nowadays, edible insects have been regarded as a promising alternative food resources in many regions of the world by virtue of their nutritive values (e.g., high protein content, sufficient minerals), socioeconomic advantages (e.g., requirement of less cost, water and space in insect farming compared to livestock farming), and environmental benefits (e.g., less emission of greenhouse gases and ammonia in insect farming) (Govorushko, 2019). Bean worm (*Clanis bilineata*) larva, which is widely consumed in North Jiangsu Province of China, contains protein level of 68.5% [dry weight (dw) basis] and essential amino acid level of 52.8% (dw), both of which are greater than those of milk and eggs (Xia et al., 2012). In China, more than 10,000 tons of bean worms are consumed every year, and about 2000 tons of skin waste is generated, which is often indiscriminately disposed of, potentially causing environment problems (e.g., pathogen, stench) (Yan et al., 2020). Hence, it is of urgency and significance to dispose the waste bean worm skin safely, and in economically viable way.

Traditional methods of animal carcass and waste disposal (e.g., burial, incineration and composting) present significant limitations, such as release of infectious agents into the surface and ground water, emission of gaseous pollutants, and long processing time (Gwyther et al., 2011; Zhang et al., 2018). In comparison, pyrolysis can effectively destroy pathogens, shorten the waste processing time, and produce clean energy (e.g., bio-oil, syngas) and stable biochar. Pyrolysis has thus been regarded as a promising alternative technology for the disposal of animal carcasses and wastes (Chen et al., 2020; Gwyther et al., 2011; Zhang et al., 2018). Recent studies have demonstrated that conversion of biomass feedstocks to biochar could generate large specific surface area (SSA), active sorption sites, and modified surface electric charge, thus facilitating sorption of heavy metals (Cao et al., 2019). For example, Lee et al. (2015)

reported that the maximum adsorption amount of Pb(II) on peat moss increased by 10.6% after converting the feedstock to biochar via pyrolysis. Amin (2018) showed that the maximum adsorption amount of Pb(II) on banana peel derived biochar (227.27 mg g^{-1}) was significantly greater than raw banana peel (2.18 mg g^{-1}) (Anwar et al., 2010). Cao et al. (2019) found ten-fold large SSA of wheat straw after pyrolysis, and that adsorption capacity of wheat straw increased from 46.33 to 119.55 mg g^{-1} .

Therefore, the overall aim of this work is to convert the bean worm skin waste (BWS) into a high-value biochar (BWS-BC), and to investigate the difference of adsorption properties between BWS and BWS-BC toward aqueous Pb(II). Specifically, the effects of pH, contact time, input Pb(II) concentration and temperature on Pb(II) adsorption were investigated by batch experiments. Subsequently, several classical adsorption models (e.g., kinetic and isotherm) were studied for understanding the Pb(II) adsorption process in depth. Furthermore, appropriate characterization techniques were employed to investigate the mechanism that were responsible for the adsorption of Pb(II) on the studied adsorbents.

2. Materials and methods

2.1. Materials

BWS samples were obtained from a farmers' market in North Jiangsu Province, China. Before using, the samples were subjected to stepwise pretreatment processes, comprising rinsed with tap water, air-dried to constant weight, and ground to less than 0.15 mm powder. BWS-BC was prepared by pyrolyzing the pre-treated BWS powder at $500 \text{ }^{\circ}\text{C}$ for 4 h under oxygen limited condition in a quartz tube furnace with a heating rate of $5 \text{ }^{\circ}\text{C min}^{-1}$.

A simulated wastewater containing 1000 mg L^{-1} Pb(II) was prepared by dissolving the

accurate amount of $\text{Pb}(\text{NO}_3)_2$ to deionized water. The desired $\text{Pb}(\text{II})$ concentrations in the subsequent experiments were obtained by diluting the simulated wastewater using deionized water. All chemical reagents (analytical grade) used in this study (e.g., NaOH , NaCl , HNO_3) were obtained from Sinopharm Chemical Reagent Co. Ltd., Shanghai, China.

2.2. Characterization

The zeta potential values of BWS and BWS-BC were measured by Zetasizer (Nano series, Malvern, England). The information on functional groups, surface morphology and mineral composition of the two adsorbents pre- and post- $\text{Pb}(\text{II})$ adsorption was determined by Fourier-transform infrared spectroscopy (FTIR, Nicolet is50, Thermo Scientific, USA), scanning electron microscopy linked to energy dispersive spectroscopy (SEM-EDS, Quanta 250FEG, FEI, USA), and X-ray diffraction (XRD, EPSILON5, PANalytical, Netherlands), respectively. The $\text{Pb}(\text{II})$ concentration in solutions was determined via inductively coupled plasma optical emission spectrometry (ICP-OES, Optima 7000DV, PerkinElmer, USA). In addition, the basic physicochemical properties, including the pH, ash contents, cation exchange capacity (CEC), elemental contents (C, N, H, O and P) and SSA of BWS and BWS-BC were determined by the methods described in our previous work (Yan et al., 2020), and the results are shown in Table S1 (Supplementary Materials).

2.3. Batch experiments

Batch adsorption experiments were conducted in 50 mL Corning centrifuge tubes with a mixture of 0.05 g adsorbent and 30 mL $\text{Pb}(\text{II})$ -containing solution (0.01 mol L^{-1} NaCl as the background electrolyte to maintain the ionic strength) on a rotating shaker at constant rotating speed of 200 rpm. The adsorption amount of $\text{Pb}(\text{II})$ at time t (q_t , mg g^{-1}) was calculated

according to:

$$q_t = \frac{(C_0 - C_t)V}{m} \quad (1)$$

where, C_0 (mg L^{-1}) is the initial Pb(II) concentration; C_t (mg L^{-1}) is the Pb(II) concentration at time t ; V (L) is the volume of Pb(II)-containing solution; m (g) is the weight of BWS and BWS-BC.

To investigate the effect of pH (2.0 ~ 6.0) on adsorption, each adsorbent was mixed with 100 mg Pb(II) L^{-1} solution at 25 °C for 24 h, and the initial pH value of the solution was adjusted using 0.1 mol L^{-1} NaOH and 0.1 mol L^{-1} HNO₃. To avoid the interference induced from Pb hydroxide species, the pH range of 2.0 ~ 6.0 was selected in this study. The kinetic experiments were carried out by adding each adsorbent into 100 mg Pb(II) L^{-1} solution (pH 5.0 ± 0.2) at 25 °C, relevant centrifuge tubes were withdrawn at the stated intervals of 5 ~ 1440 min. The equilibrium experiments were performed by mixing adsorbents with various Pb(II) concentrations (20 ~ 300 mg L^{-1} , pH 5.0 ± 0.2) at 25 °C for 24 h. Adsorption thermodynamic behavior was studied at different reaction temperatures (10 ~ 40 °C) at pH 5.0 ± 0.2 for 24 h. After adsorption, the suspension was promptly filtered by 0.22 μm membrane filters, and the filtrate was collected and diluted for determination of residual Pb(II) concentration. All experiments were performed in triplicate, and mean results are presented.

3. Results and discussion

3.1. Effect of pH

Solution pH can affect both the surface charge of adsorbents and chemical speciation of heavy metal ions, leading to the change in adsorption performance. The model established using Visual MINTEQ software (Fig. 1a) showed that Pb(II) was the primary species in the pH range

of 2.0 ~ 6.0. The effect of solution pH on Pb(II) adsorption by BWS and BWS-BC is shown in Fig. 1b. The adsorption of Pb(II) on BWS and BWS-BC was both pH dependent, but the impact extent was different. The adsorption amount of BWS increased significantly with raising pH from 2.0 to 5.0, and then tended to remain constant. The Pb(II) adsorption amount of BWS-BC had a slight fluctuation at pH values > 3.0, implying a good buffering capacity for BWS-BC. Moreover, the amount of Pb(II) adsorbed on BWS-BC (26.4 ~ 45.8 mg g⁻¹) was higher than that of BWS (11.2 ~ 33.4 mg g⁻¹) over the entire pH range. These phenomena could be attributed to the following three reasons (Rwiza et al., 2018; Yan et al., 2015). Initially, the relatively low pH condition caused competition between proton and Pb(II) for the confined active sites on the surface of adsorbents. Moreover, the partial dissolution of adsorbents at highly acidic environment led to the reduction in surface active sites. Finally, as shown in Fig. 1b, the points of zero charge (pH_{pzc}) of BWS and BWS-BC were 3.4 and 2.1, respectively. At pH < 3.4, an electrostatic repulsion inhibited the adsorption of positively charged Pb(II) on the positively charged surface of BWS. As pH values increased, the negatively charged sites on the surface of BWS enhanced gradually, thus the strong electrostatic attraction occurred, which was favorable to Pb(II) adsorption. A similar explanation was also valid for the case of BWS-BC. Notably, all zeta potentials of BWS-BC were much lower than that of BWS, indicating that BWS-BC possessed a higher binding ability to Pb(II) compared to BWS.

3.2. Adsorption kinetics

Fig. 2 shows the effect of contact time on Pb(II) adsorbed by BWS and BWS-BC. It was apparent that the adsorption curves increased steeply within first 60 min, which indicated that abundant adsorption sites on the external surface of adsorbents were rapidly occupied by Pb(II)

via physisorption (Ahmad et al., 2014; Wang et al., 2015; Xiao et al., 2017). As time proceeded, the adsorption curves increased slowly, and finally reached a pseudo equilibrium within 960 and 480 min for BWS and BWS-BC, respectively. This may be ascribed to the irreversible chemisorption toward the end of the adsorption process (Ahmad et al., 2014; Wang et al., 2015; Xiao et al., 2017). To better understand the rate-controlling steps responsible for Pb(II) adsorption on BWS and BWS-BC, the pseudo-first order and pseudo-second order kinetic models (Ho et al., 1996; Li et al., 2007) were explored to fit the experimental data. The linearized equations of the above models were presented in Supplementary Materials.

The fitted parameters of kinetic models at 25 °C are presented in Table S2. The coefficients of determination (R^2) predicted by the pseudo-second order model for BWS (0.9982) and BWS-BC (0.9999) were both higher than those of the pseudo-first order model (0.9613 and 0.9103 for BWS and BWS-BC, respectively). Furthermore, the theoretical adsorption capacities ($q_{e, cal}$) predicted from the pseudo-second order model was 33.78 and 45.05 mg g⁻¹ for BWS and BWS-BC, respectively, which were in good agreement with the values obtained in this study (32.82 and 43.98 mg g⁻¹ for BWS and BWS-BC, respectively). These results suggested that the adsorption data of Pb(II) on both adsorbents could be suitably represented by the pseudo-second order model, implying that the rate-limiting steps over two adsorption processes were controlled by chemisorption. Similar results were obtained by Zhou et al. (2018) who revealed that the adsorption process of Cu(II) and Cd(II) by ferromanganese binary oxide–biochar composites was also well-described by the pseudo-second order model. In addition, the calculated initial adsorption rate (h) values followed the order of BWS-BC (1.66 mg g⁻¹ min⁻¹) > BWS (0.55 mg g⁻¹ min⁻¹), indicating that the pyrolysis of BWS could significantly enhance the initial

adsorption rate of BWS-BC toward Pb(II).

3.3. Adsorption isotherms

Fig. 3a shows the effect of equilibrium concentrations on Pb(II) adsorption by BWS and BWS-BC. When $C_e < 45 \text{ mg L}^{-1}$, the amounts of Pb(II) adsorbed on the adsorbents were found to increase remarkably. This could be ascribed to the sufficient active sites on the surface of the adsorbents during this period. On the other hand, as the values of C_e continued to increase, available active adsorption sites on the surface of the adsorbents tended to saturate, therefore resulting in a dynamic equilibrium of adsorption capacity for each adsorbent. Similar observation was reported by Cheng et al. (2016). To further explore the adsorption process of Pb(II) on BWS and BWS-BC, three classical isotherm models including the Langmuir, Freundlich and Dubinin-Radushkevich (D-R) (Gorgievski et al., 2013; Kapnisti et al., 2018; Yan et al., 2020) models were employed to simulate the experimental data. The linearized forms of these models were shown in Supplementary Materials.

The fitting curves of BWS and BWS-BC are plotted in Fig. 3b ~ Fig. 3d, and their related parameters are presented in Table S3. The Langmuir model exhibited the best fit for both the adsorbents with the highest coefficients of determination ($R^2 > 0.99$). The Langmuir model is associated with a fixed number of identical and energetically equivalent active sites on the homogeneous surface of adsorbents (Yan et al., 2015). Hence, it could be inferred that there was no lateral interaction between Pb(II) and the adsorbents, i.e., the adsorption energy level to Pb(II) was uniformly distributed on the surface of BWS and BWS-BC. The maximum adsorption capacities (q_{\max}) of BWS and BWS-BC toward Pb(II) were 45.45 and 61.73 mg g^{-1} , respectively, which were comparable with other similar adsorbents (Table S4), indicating a

good potential application of BWS-BC in practical wastewater treatment. The separation factor (R_L) (Supplementary Materials) plays an important role in evaluating the favorability of adsorption. The adsorption is favorable when $0 < R_L < 1$, while $R_L = 1$, $R_L > 1$ and $R_L = 0$ correspond to linear, unfavorable and irreversible adsorption, respectively (Xiong et al., 2019). The R_L values for BWS and BWS-BC were calculated as $0.04 \sim 0.37$ and $0.02 \sim 0.28$, respectively, where all values fell within the range of $0 \sim 1$, confirming the favorable adsorption of Pb(II) on BWS and BWS-BC. Notably, the R_L values of BWS-BC were much smaller than those of BWS, indicating a higher binding affinity between Pb(II) and BWS-BC (Zhou et al., 2018).

Additionally, the $1/n$ and K_F obtained from the Freundlich equation could be the indicators of adsorption favorability, such as $0 < 1/n < 1$ indicates a favorable adsorption (Yan et al., 2020). In this study, the $1/n$ values of BWS and BWS-BC ranged between 0 to 0.3, indicating favorable adsorption of Pb(II) by the two adsorbents (Ding et al., 2016). The K_F values followed the order: BWS-BC $>$ BWS, also suggesting a relatively stronger cohesive force between BWS-BC and Pb(II), i.e., the pyrolysis of BWS could significantly enhance the adsorption affinity toward Pb(II).

The mean free energy constant (E) predicted from the D-R equation could give important information about the adsorption mechanisms, such as physical adsorption when $E < 8$ kJ/mol, and chemical adsorption when $E > 8$ kJ/mol (Ding et al., 2016). In the present study, the values of E were 14.67 and 15.52 kJ mol⁻¹ for BWS and BWS-BC, respectively. Both these values exceeded 8 kJ mol⁻¹, indicating that the adsorption of Pb(II) on BWS and BWS-BC took place chemically, which was consistent with the results of the pseudo-second order model fitting of

the kinetic data.

3.4. Adsorption thermodynamics

Analysis of thermodynamic parameters not only judges the nature of adsorption process, but also obtains the information on predominant mechanisms occurring in the adsorption reaction (e.g., physical interaction, chemical interaction) (Rahmani-Sani et al., 2020). In the present study, thermodynamic parameters including Gibbs free energy change (ΔG° , kJ mol⁻¹), enthalpy change (ΔH° , kJ mol⁻¹) and entropy change (ΔS° , kJ mol⁻¹ K⁻¹) were calculated from the Van't Hoff equation (shown in Supplementary Materials) at 283, 298 and 313 K temperatures.

The corresponding thermodynamic parameters are listed in Table S5. The ΔG° values negatively increased from -0.28 to -9.56 kJ mol⁻¹ and -4.31 to -20.84 with temperature rose from 283 to 313 K for BWS and BWS-BC, respectively. These results indicated that the adsorption of Pb(II) on BWS and BWS-BC was thermodynamically favorable and highly spontaneous at high working temperature. The positive ΔH° values were indicators of the endothermic nature for Pb(II) adsorption on BWS and BWS-BC. According to ΔH° values, the adsorption types could be identified as physical adsorption ($2.1 < \Delta H^\circ < 20.9$ kJ mol⁻¹) and chemical adsorption ($20.9 < \Delta H^\circ < 418.4$ kJ mol⁻¹) (Yan et al., 2015). The obtained ΔH° values for BWS (86.84 kJ mol⁻¹) and BWS-BC (149.74 kJ mol⁻¹) ranged from 20.9 to 418.4 kJ mol⁻¹, indicating chemical interaction taking place between Pb(II) and the adsorbents, which was in accord with the kinetic and isotherm results. The positive ΔS° values for BWS (0.31 kJ mol⁻¹ K⁻¹) and BWS-BC (0.54 kJ mol⁻¹ K⁻¹) suggested an increased extent of randomness at the interfaces of Pb(II)-BWS and Pb(II)-BWS-BC, which could facilitate the adsorption. Interestingly, the absolute values of all the thermodynamic data for BWS-BC were greater than that of BWS, reflecting that the

adsorption feasibility, favorability and spontaneity for BWS to Pb(II) could be significantly enhanced by pyrolysis.

3.5. Possible adsorption mechanism

The surface functional group information of the adsorbents pre- and post-Pb(II) adsorption is presented in Fig. 4. For BWS, the broad FTIR bands in the range of 3280 ~ 3430 cm^{-1} were attributed to the stretching vibrations of O-H and N-H groups (Wu et al., 2017). The bands at 2928 and 1315 cm^{-1} were associated with the stretching vibrations of C-H and N-H bonds, respectively (Ali et al., 2020; Fernández-López et al., 2019). The bands at 1650 and 1542 cm^{-1} were corresponding to amide I (band of C=O stretching vibration) and amide II (bands of C-N stretching vibration and N-H bending vibration), respectively (Saravana et al., 2018). The band at 1446 cm^{-1} was assigned to the out-of-plane bending vibration for carbonates (Lee et al., 2019; Xu et al., 2013). The bands at 1387 and 1251 cm^{-1} were ascribed to the deformation vibrations of C-H and O-H bonds, respectively (Gao et al., 2020; Wu, 2012). The special absorption bands observed at 1155 and 895 cm^{-1} represented the β (1 \rightarrow 4) glycosidic bond (Wu et al., 2017). The bands at 1110, 1070 and 570 cm^{-1} indicated the occurrence of P-O bond (Lee et al., 2019; Lei et al., 2019). After Pb(II) adsorption, the characteristic spectral bands at 1251, 1387, 1542 and 570 cm^{-1} were shifted to 1235, 1378, 1538 and 476 cm^{-1} , respectively, indicative of the participation of O-H, C-H, N-H, C-N, and P-O bonds in adsorption of Pb(II) on BWS. For BWS-BC, most of the characteristic IR bands in BWS disappeared and/or weakened, meanwhile, a new intense band emerged at 1582 cm^{-1} , which was characteristic of C=C bond in aromatic ring (Gao et al., 2020). In addition, the stronger bands at 3421 (phenolic O-H bond) and 1111 (P-O bond) cm^{-1} for BWS-BC compared to that of BWS indicated the reinforcement

of aromatization degree and P exposure of BWS owing to pyrolysis reaction. In the case of BWS-BC loaded with Pb(II), a significant shift was observed on P-O bond at 1109 to 1087 cm^{-1} region, and a new characteristic adsorption band of P-O bond occurred at 476 cm^{-1} , both implying the importance of P in Pb(II) adsorption on BWS-BC. As shown in Table S1, BWS-BC had higher P content than BWS, which might have facilitated a greater Pb adsorption by BWS-BC over BWS.

The SEM images of two adsorbents before and after Pb(II) adsorption are shown in Fig. 5. It was observed that BWS possessed a laminated structure with a relatively smooth surface (Fig. 5a). As seen from Fig. 5d, the presence of rough surfaces on the laminated structure of BWS-BC was due to partial decomposition of the organic components in BWS after pyrolysis (Shen et al., 2019), which also was an evidence of the increase in SSA (Table S1). After Pb(II) adsorption, the laminated structures were converted into a lot of fragments in both BWS and BWS-BC (Fig. 5b and e). Meanwhile, numerous rod-shaped crystallites were generated and aggregated on the surface of the adsorbents (Fig. 5c and f). Furthermore, the EDS spectra (inset in Fig. 5c and f) showed that the fine crystallites primarily consisted of C, Pb O, P, and Si. The XRD results of the post-adsorption samples, as illustrated in Fig. 6, confirmed this observation. New characteristic diffraction reflections were indexed to the precipitation of Pb-P-O, Pb-C-O and Pb-Si-O compounds. The emergence of hydroxypyromorphite ($\text{Pb}_5(\text{PO}_4)_3\text{OH}$), hydrocerussite ($\text{Pb}_3(\text{CO}_3)_2(\text{OH})_2$) and alamosite (PbSiO_3) was noticed for the post-adsorption BWS-BC sample, while only hydroxypyromorphite was involved in the case of BWS. Overall, the pyrolysis could significantly enhance the exposure of active sites (e.g., P, Si) in BWS, which played the primary role in Pb(II) adsorption on BWS-BC.

4. Conclusions

Pyrolysis was proved to be an effective approach in improving the adsorption performance of BWS toward Pb(II). In comparison with BWS, the good buffering ability of BWS-BC due to the higher pH value of the later adsorbent than the former led to the less fluctuation of pH values in the adsorption system (initial pH = 2.0 to 6.0). Also, the reduction in zeta potentials for BWS-BC strengthened the electrostatic attraction of the adsorbent to solution Pb(II). The results of adsorption kinetics showed a faster initial adsorption rate for BWS-BC ($1.66 \text{ mg g}^{-1} \text{ min}^{-1}$) than BWS ($0.55 \text{ mg g}^{-1} \text{ min}^{-1}$). The maximum adsorption capacities calculated from the Langmuir isotherm equation were 45.45 and 61.73 mg g^{-1} , respectively, which are highly competitive with other similar adsorbents. The thermodynamic study suggested that both BWS and BWS-BC could favorably, spontaneously and endothermically adsorb solution Pb(II). Moreover, pyrolysis could significantly enhance the exposure of surface active sites of BWS, thus enhancing the Pb(II) adsorption. Specially, BWS-BC could intensely adsorb solution Pb(II) through precipitation of hydroxypyromorphite, hydrocerussite and alamosite, while forming hydroxypyromorphite for BWS.

Acknowledgments

The authors would like to acknowledge the National Natural Science Foundation of China (41907133), Jiangsu Provincial Natural Science Foundation (BK20191057, HAB201827), National Key Research and Development Program of China (2018YFD0800305, 2016YFD0800400), Agricultural Science and Technology Innovation Program of Chinese Academy of Agricultural Sciences (2018-2021), China Postdoctoral Science Foundation (2018M641557), Jiangsu Provincial Natural Science Foundation for Universities

(19KJD610002), and Open Funds of Provincial Laboratories (JSEFM201808, BEETKC1906) for their financial support.

References

- Ahmad, M., Rajapaksha, A.U., Lim, J.E., Zhang, M., Bolan, N., Mohan, D., Vithanage, M., Lee, S.S., Ok, Y.S., 2014. Biochar as a sorbent for contaminant management in soil and water: a review. *Chemosphere* 99, 19-33.
- Ali, S., Rizwan, M., Shakoor, M.S., Jilani, A., Anjum, R., 2020. High sorption efficiency for As(III) and As(V) from aqueous solutions using novel almond shell biochar. *Chemosphere* 243, 125330.
- Amin, M.T., Alazba, A.A., Shafiq, M., 2018. Removal of copper and lead using banana biochar in batch adsorption systems: Isotherms and kinetic studies. *Arab. J. Sci. Eng.* 43, 5711-5722.
- Anastopoulos, I., Pashalidis, I., Hosseini-Bandegharai, A., Giannakoudakis, D.A., Robalds, A., Usman, M., Escudero, L.B., Zhou, Y., Colmenares, J.C., Núñez-Delgado, A., Lima, E.C., 2019. Agricultural biomass/waste as adsorbents for toxic metal decontamination of aqueous solutions. *J. Mol. Liq.* 295, 111684.
- Anwar, J., Shafique, U., Waheed-uz-Zaman, Salman, M., Dar, A., Anwar, S., 2010. Removal of Pb(II) and Cd(II) from water by adsorption on peels of banana. *Bioresource Technol.* 101, 1752-1755.
- Cao, Y., Xiao, W., Shen, G., Ji, G., Zhang, Y., Gao, C., Han, L., 2019. Carbonization and ball milling on the enhancement of Pb(II) adsorption by wheat straw: Competitive effects of ion exchange and precipitation. *Bioresource Technol.* 273, 70-76.

- Chen, H., Yang, X., Wang, H., Sarkar, B., Shaheen, S.M., Gielen, G., Bolan, N., Guo, J., Che, L., Sun, H., Rinklebe, J., 2020. Animal carcass- and wood-derived biochars improved nutrient bioavailability, enzyme activity, and plant growth in metal-phthalic acid ester co-contaminated soils: A trial for reclamation and improvement of degraded soils. *Journal of Environmental Management* 261, 110246.
- Cheng, Q., Huang, Q., Khan, S., Liu, Y., Liao, Z., Li, G., Ok, Y.S., 2016. Adsorption of Cd by peanut husks and peanut husk biochar from aqueous solutions. *Ecol. Eng.* 87, 240-245.
- Ding, Z., Wan, Y., Hu, X., Wang, S., Zimmerman, A.Z., Gao, B., 2016. Sorption of lead and methylene blue onto hickory biochars from different pyrolysis temperatures: Importance of physicochemical properties. *J. Ind. Eng. Chem.* 37, 261-267.
- Fernández-López, J.A., Fernández-López, J.M., Roca, M.J., Miñarro, M.D., 2019. Taguchi design-based enhancement of heavy metals bioremoval by agroindustrial waste biomass from artichoke. *Sci. Total Environ.* 653, 55-63.
- Gao, R., Xiang, L., Hu, H., Fu, Q., Zhu, J., Liu, Y., Huang, G., 2020. High-efficiency removal capacities and quantitative sorption mechanisms of Pb by oxidized rape straw biochars. *Sci. Total Environ.* 699, 134262.
- Gorgievski, M., Božić, D., Stanković, V., Štrbac, N., Šerbula, S., 2013. Kinetics, equilibrium and mechanism of Cu^{2+} , Ni^{2+} and Zn^{2+} ions biosorption using wheat straw. *Ecol. Eng.* 58, 113-122.
- Govorushko, S., 2019. Global status of insects as food and feed source: A review. *Trends Food Sci. Tech.* 91, 436-445.
- Gwyther, C.L., Williams, A.P., Golyshin, P.N., Edwards-Jones, G., Jones, D.L., 2011. The

- environmental and biosecurity characteristics of livestock carcass disposal methods: A review. *Waste Manage.* 31, 767-778.
- Ho, Y.S., Wase, D.A.J., Forster, C.F., 1996. Kinetic studies of competitive heavy metal adsorption by sphagnum moss peat. *Environ. Technol.* 17, 71-77.
- Lee, M., Park, J.H., Chung, J.W., 2019. Comparison of the lead and copper adsorption capacities of plant source materials and their biochars. *J. Environ. Manage.* 236, 118-124.
- Lee, S., Park, J.H., Ahn, Y., Chung, J.W., 2015. Comparison of heavy metal adsorption by peat moss and peat moss-derived biochar produced under different carbonization conditions. *Water Air Soil Poll.* 226, 9.
- Lei, S., Shi, Y., Qiu, Y., Che, L., Xue, C., 2019. Performance and mechanisms of emerging animal-derived biochars for immobilization of heavy metals. *Sci. Total Environ.* 646, 1281-1289.
- Li, Q., Zhai, J., Zhang, W., Wang, M., Zhou, J., 2007. Kinetic studies of adsorption of Pb(II), Cr(III) and Cu(II) from aqueous solution by sawdust and modified peanut husk. *J. Hazard. Mater.* 141, 163-167.
- Lingamdinne, L.P., Yang, J., Chang, Y., Koduru, J.R., 2016. Low-cost magnetized *Lonicera japonica* flower biomass for the sorption removal of heavy metals. *Hydrometallurgy* 165, 81-89.
- Kapnisti, M., Noli, F., Misaelides, P., Vourlias, G., Karfaridis, D., Hatzidimitriou, A., 2018. Enhanced sorption capacities for lead and uranium using titanium phosphates; sorption, kinetics, equilibrium studies and mechanism implication. *Chem. Eng. J.* 342, 184-195.
- Rahmani-Sani, A., Singh, P., Raizada, P., Lima, E.C., Anastopoulos, I., Giannakoudakis, D.A.,

- Sivamani, S., Dontsova, T.A., Hosseini-Bandegharaei, A., 2020. Use of chicken feather and eggshell to synthesize a novel magnetized activated carbon for sorption of heavy metal ions. *Bioresource Technol.* 297, 122452.
- Rwiza, M.J., Oh, S., Kim, K., Kim, S.D., 2018. Comparative sorption isotherms and removal studies for Pb(II) by physical and thermochemical modification of low-cost agro-wastes from Tanzania. *Chemosphere* 195, 135-145.
- Saravana, P.S., Ho, T.C., Chae, S., Cho, Y., Park, J., 2018. Deep eutectic solvent-based extraction and fabrication of chitin films from crustacean waste. *Carbohydr. Polym.* 195, 622-630.
- Semerjian, L., 2018. Removal of heavy metals (Cu, Pb) from aqueous solutions using pine (*Pinus halepensis*) sawdust: Equilibrium, kinetic, and thermodynamic studies. *Environ. Technol. Inno.* 12, 91-103.
- Shen, Z., Hou, D., Jin, F., Shi, J., Fan, X., Tsang, D.C.W., Alessi, D.S., 2019. Effect of production temperature on lead removal mechanisms by rice straw biochars. *Sci. Total Environ.* 655, 751-758.
- Vilardi, G., Palma, L.D., Verdone, N., 2018. Heavy metals adsorption by banana peels micro-powder: Equilibrium modeling by non-linear models. *Chinese J. Chem. Eng.* 26, 455-464.
- Wang, S., Gao, B., Li, Y., Mosa, A., Zimmerman, A.R., Ma, L.Q., Harris, W.G., Migliaccio, K.W., 2015. Manganese oxide-modified biochars: Preparation, characterization, and sorption of arsenate and lead. *Bioresource Technol.* 181, 13-17.
- Wierzba, S., Kłós, A., 2019. Heavy metal sorption in biosorbents – Using spent grain from the brewing industry. *J. Clean. Prod.* 225, 112-120.

- Wu, S., 2012. Preparation of chitooligosaccharides from *Clanis bilineata* larvae skin and their antibacterial activity. *Int. J. Biol. Macromol.* 51, 1147-1150.
- Wu, S., Lu, M., Wang, S., 2017. Antiageing activities of water-soluble chitosan from *Clanis bilineata* larvae. *Int. J. Biol. Macromol.* 102, 376-379.
- Xia, Z., Wu, S., Pan, S., Kim, J.M., 2012. Nutritional evaluation of protein from *Clanis bilineata* (Lepidoptera), an edible insect. *J. Sci. Food Agric.* 92, 1479-1482.
- Xiao, Y., Xue, Y., Gao, F., Mosa, A., 2017. Sorption of heavy metal ions onto crayfish shell biochar: Effect of pyrolysis temperature, pH and ionic strength. *J. Taiwan Inst. Chem. E.* 80, 114-121.
- Xiong, C., Wang, S., Sun, W., Li, Y., 2019. Selective adsorption of Pb(II) from aqueous solution using nanosilica functionalized with diethanolamine: Equilibrium, kinetic and thermodynamic. *Microchem. J.* 146, 270-278.
- Xu, X., Cao, X., Zhao, L., 2013. Comparison of rice husk- and dairy manure-derived biochars for simultaneously removing heavy metals from aqueous solutions: Role of mineral components in biochars. *Chemosphere* 92, 955-961.
- Yan, Y., Li, Q., Sun, X., Ren, Z., He, F., Wang, Y., Wang, L., 2015. Recycling flue gas desulphurization (FGD) gypsum for removal of Pb(II) and Cd(II) from wastewater. *J. Colloid Interface Sci.* 457, 86-95.
- Yan, Y., Zhang, L., Wang, Y., Wang, X., Wang, S., Li, Q., Liu, X., Xu, Y., Yang, J., Bolan, N., 2020. *Clanis bilineata* larvae skin-derived biochars for immobilization of lead: Sorption isotherm and molecular mechanism. *Sci. Total Environ.* 704, 135251.
- Zhang, Y., Ma, Z., Yan, J., 2018. Influence of pork and bone on product characteristics during

the fast pyrolysis of pig carcasses. *Waste Manage.* 75, 352-360.

Zhou, Q., Liao, B., Lin, L., Qiu, W., Song, Z., 2018. Adsorption of Cu(II) and Cd(II) from aqueous solutions by ferromanganese binary oxide–biochar composites. *Sci. Total Environ.* 615, 115-122.

Figure captions

Fig. 1 (a) The distribution of Pb species in solution ionic strength of 0.01 mol/L NaNO₃ at 25 °C, and (b) the effect of pH on Pb(II) adsorption and the surface zeta potential curves of BWS and BWS-BC.

Fig. 2 The effect of contact time on Pb(II) adsorption on BWS and BWS-BC.

Fig. 3 (a) The effect of equilibrium adsorbate concentration on Pb(II) adsorption on BWS and BWS-BC, (b) Langmuir fit curves, (c) Freundlich fit curves, and (d) D-R fit curves.

Fig. 4 FTIR spectra of BWS and BWS-BC before and after Pb(II) adsorption.

Fig. 5 SEM-EDS images of (a) BWS, (b-c) BWS after Pb(II) adsorption, (d) BWS-BC, and (e-f) BWS-BC after Pb(II) adsorption.

Fig. 6 XRD patterns of BWS and BWS-BC before and after Pb(II) adsorption.

Figures

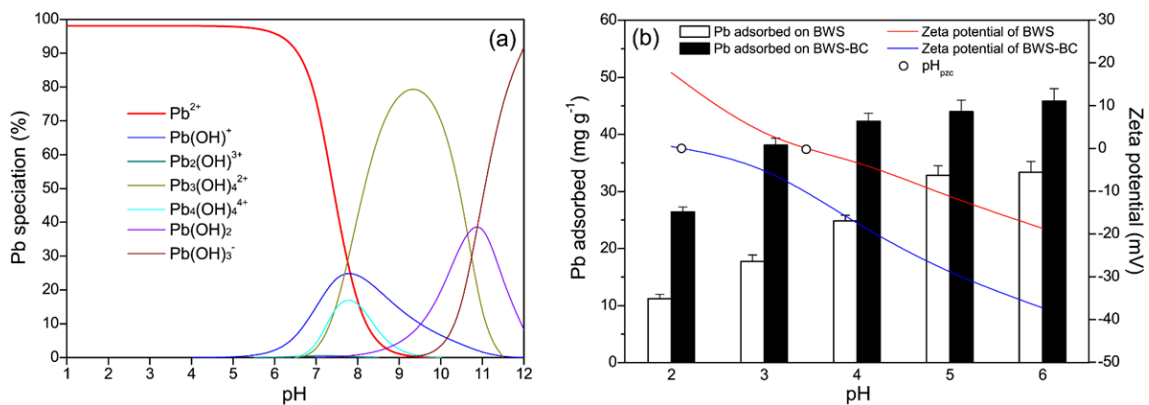


Fig. 1

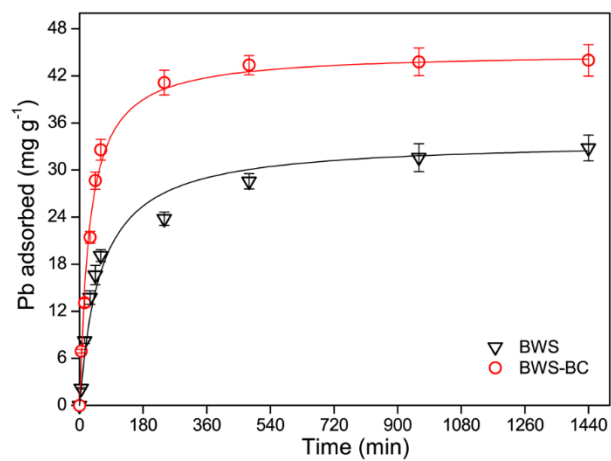


Fig. 2

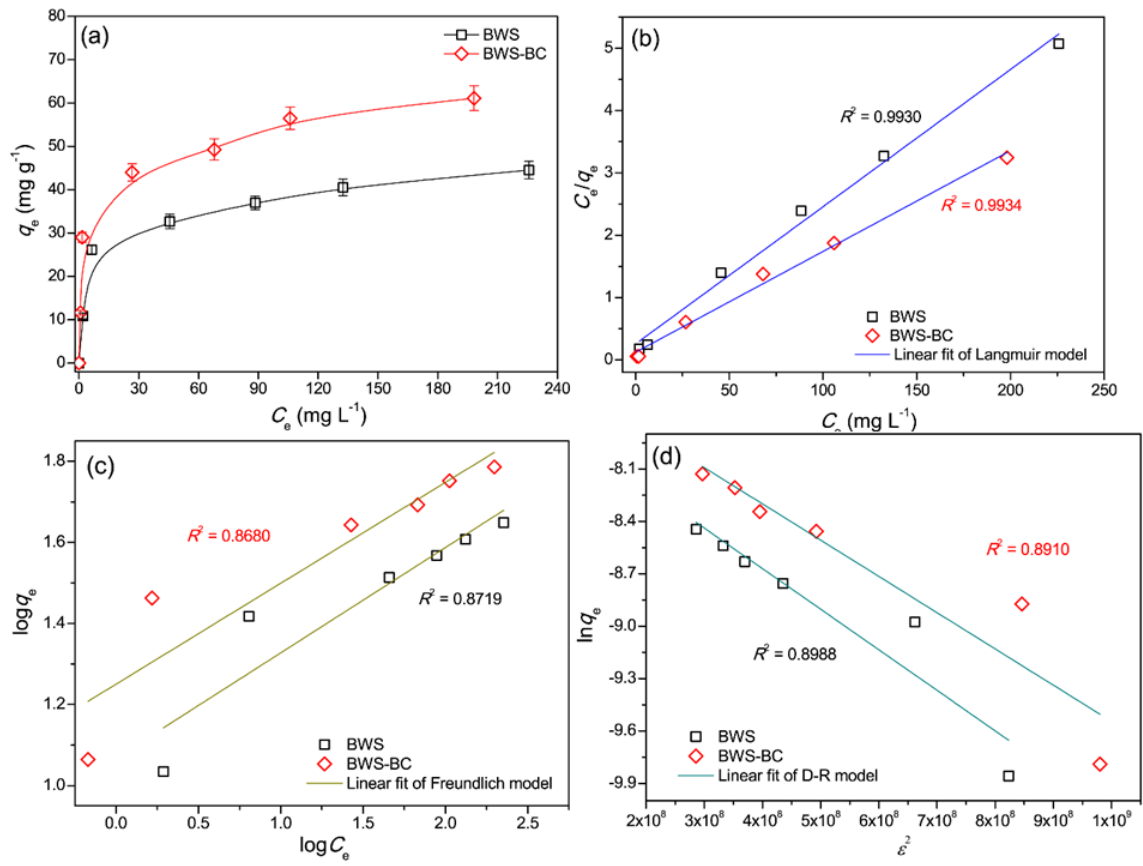


Fig. 3

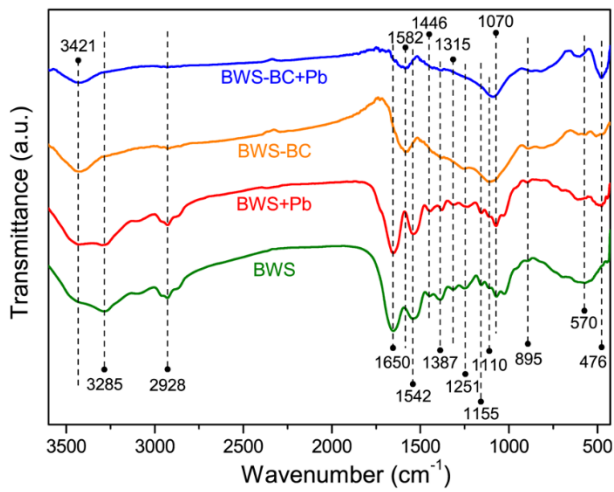


Fig. 4

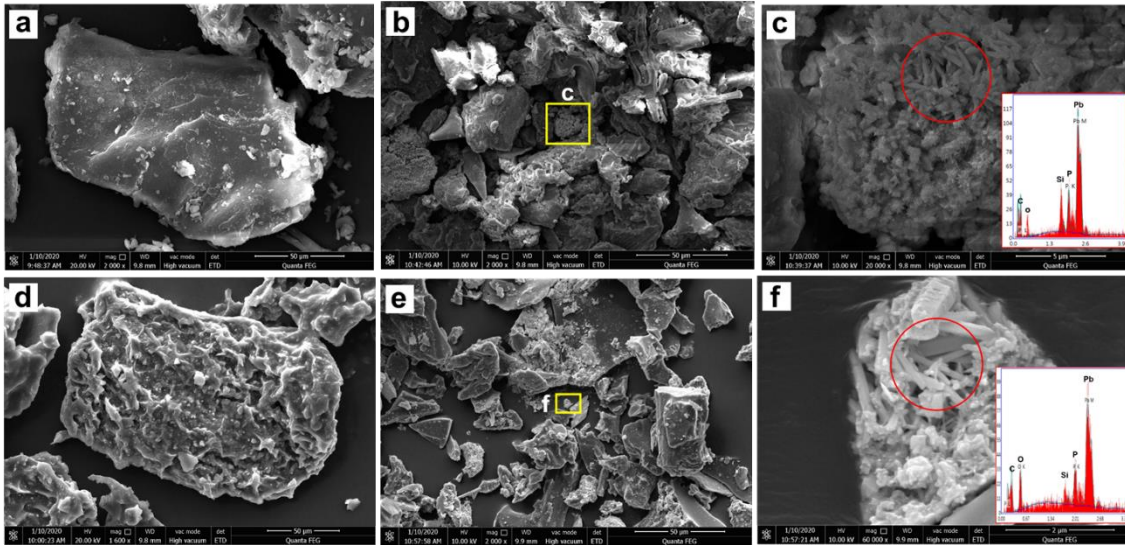


Fig. 5

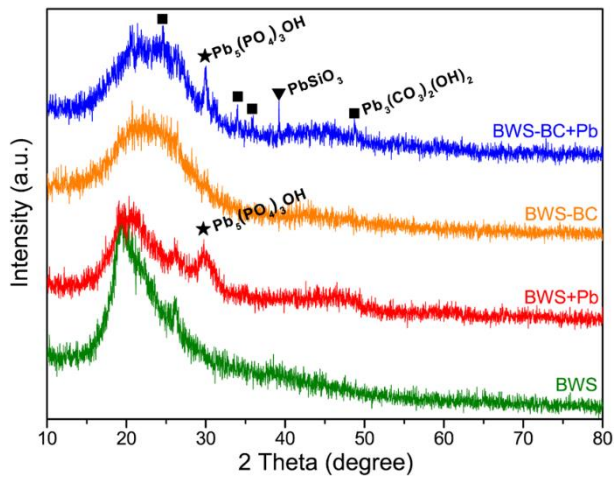


Fig. 6

Supplementary Materials for

**Phosphorus-rich biochar produced through bean-worm skin waste
pyrolysis enhances the adsorption of aqueous lead**

Yubo Yan^{a,b}, Binoy Sarkar^c, Lei Zhou^a, Ling Zhang^d, Qiao Li^e, Jianjun Yang^{b*}, Nanthi Bolan^{f,g}

^a*School of Chemistry and Chemical Engineering, Huaiyin Normal University, Huai'an 223300, China*

^b*Institute of Environmental and Sustainable Development in Agriculture, Chinese Academy of Agricultural Science, Beijing 100081, China*

^c*Lancaster Environment Centre, Lancaster University, Lancaster, LA1 4YQ, United Kingdom*

^d*School of Health, Jiangsu Food & Pharmaceutical Science College, Huai'an 223001, China*

^e*School of Environmental and Biological Engineering, Nanjing University of Science and Technology, Nanjing 210094, China*

^f*Global Centre for Environmental Remediation, University of Newcastle, Callaghan Campus, NSW 2308, Australia*

^g*Cooperative Research Centre for High Performance Soil (Soil CRC), Callaghan, NSW 2308, Australia*

Linearized equations for the kinetic models

$$\text{Pseudo-first order model: } \log(q_e - q_t) = \log q_e - \frac{k_1 t}{2.303} \quad (1)$$

$$\text{Pseudo-second order model: } \frac{t}{q_t} = \frac{1}{k_2 q_e^2} + \frac{t}{q_e} \quad (2)$$

where, q_e (mg g^{-1}) is the equilibrium amount of Pb(II) adsorbed on BWS and BWS-BC; q_t (mg g^{-1}) is the amount of Pb(II) adsorbed at time t (min); k_1 (min^{-1}) and k_2 ($\text{g mg}^{-1} \text{min}^{-1}$) are relevant rate constants. What's more, as t in Eq. (2) approaches 0, the initial adsorption rate (h , $\text{mg g}^{-1} \text{min}^{-1}$) of Pb(II) on different adsorbents can be calculated by:

$$h = k_2 q_e^2 \quad (3)$$

Linearized equations for the isotherm models

$$\text{Langmuir model: } \frac{C_e}{q_e} = \frac{C_e}{q_{\max}} + \frac{1}{b q_{\max}} \quad (4)$$

$$R_L = \frac{1}{1 + b C_0} \quad (5)$$

$$\text{Freundlich model: } \log q_e = \log K_F + \frac{1}{n} \log C_e \quad (6)$$

$$\text{D-R model: } \ln q_e = \ln q_m - \beta \varepsilon^2 \quad (7)$$

$$\varepsilon = RT \ln \left(1 + \frac{1}{C_e} \right) \quad (8)$$

$$E = \frac{1}{\sqrt{2\beta}} \quad (9)$$

where, C_e (mg L^{-1}) is the equilibrium Pb(II) concentration in solution; q_e (mg g^{-1}) is the adsorption amount of BWS and BWS-BC at equilibrium; q_{\max} (mg g^{-1}) is the predicted maximum adsorption capacity of BWS and BWS-BC; q_m (mg g^{-1}) is the theoretical saturation adsorption capacity of BWS and BWS-BC; b , K_F , n and β are the constants for each model; ε and R ($8.3145 \text{ J mol}^{-1} \text{ K}^{-1}$) are the Polanyi and universal gas potentials, respectively; T (K) is Kelvin temperature; E (kJ mol^{-1}) is the mean free energy of Pb(II) adsorption on BWS and BWS-BC.

Van't Hoff equation

$$K = \frac{C_s}{C_e} \quad (10)$$

$$\Delta G^\circ = -RT \ln K \quad (11)$$

$$\ln K = \frac{\Delta S^\circ}{R} - \frac{\Delta H^\circ}{RT} \quad (12)$$

where, K is the equilibrium constant; C_s (mg g^{-1}) is the equilibrium adsorption capacity of Pb(II) on BWS and BWS-BC; C_e (mg L^{-1}) is the equilibrium Pb(II) concentration in solution.

Table S1 Selected physicochemical properties of BWS and BWS-BC.

Adsorbents	Yield (%)	pH	Ash (%)	CEC (cmol/kg)	C (%)	N (%)	H (%)	O (%)	P (mg/kg)	SSA (m ² /g)
BWS	-	5.2	4.7	0.64	43.5	14.2	10.8	29.7	6086	0.21
BWS-BC	38.4	9.4	9.6	6.9	71.2	9.7	2.1	16.6	22762	13.5

Table S2 Pseudo-first order and pseudo-second order kinetic parameters for the adsorption of Pb(II) at 25 °C.

Adsorbents	$q_{e,exp}$ (mg g ⁻¹)	Pseudo-first order kinetic			Pseudo-second order kinetic		
		k_1 (min ⁻¹)	$q_{e,cal}$ (mg g ⁻¹)	R^2	k_2 (g mg ⁻¹ min ⁻¹)	$q_{e,cal}$ (mg g ⁻¹)	R^2
BWS	32.82	3.0×10^{-3}	21.41	0.9613	4.8×10^{-4}	33.78	0.9982
BWS-BC	43.98	5.5×10^{-3}	20.98	0.9103	8.2×10^{-4}	45.05	0.9999

Table S3 Langmuir, Freundlich and Dubinin-Radushkevich isotherm parameters for the adsorption of Pb(II) at 25 °C.

Adsorbents	Langmuir			Freundlich			Dubinin-Radushkevich		
	q_{\max} (mg g ⁻¹)	b	R^2	K_F	$1/n$	R^2	q_m (mg g ⁻¹)	E (kJ mol ⁻¹)	R^2
BWS	45.45	0.0860	0.9930	11.69	0.2597	0.8719	89.94	14.67	0.8988
BWS-BC	61.73	0.1314	0.9934	17.80	0.2489	0.8680	118.1	15.52	0.8910

1 Table S4 Reported maximum adsorption capacities of Pb(II) by other adsorbents.

2

Adsorbents	q_{\max} (mg g ⁻¹)	References
<i>Raw biomasses</i>		
BWS	45.45	This study
Wheat straw	46.33	Cao et al., 2019
Peanut shell	38.91	Taşar et al., 2014
Sphagnum moss peat	30.70	Ho et al., 1996
Almond shell	26.55	Ronda et al., 2013
Sawdust	21.05	Li et al., 2007
Corn cob	16.22	Tan et al., 2010
Banana peel	2.18	Anwar et al., 2010
<i>Biochars</i>		
BWS-BC	61.73	This study
Ginkgo leaf biochar	50.62	Lee et al., 2019
Camphor leaves biochar	39.06	Wang et al., 2018
Orange peel biochar	27.86	Abdelhafez and Li, 2016
Hickory biochar	16.3	Ding et al., 2016
Peanut shell biochar	11.05	Lee et al., 2019
Rice husk biochar	2.40	Liu and Zhang, 2009
Pistachio shell biochar	1.22	Komnitsas et al., 2016

3

4

5 Table S5 Thermodynamic parameters for the adsorption of Pb(II).

6

Adsorbents	T (°C)	ΔG° (kJ mol ⁻¹)	ΔH° (kJ mol ⁻¹)	ΔS° (kJ mol ⁻¹ K ⁻¹)
BWS	10	-0.28		
	25	-3.48	86.84	0.31
	40	-9.56		
BWS-BC	10	-4.31		
	25	-7.10	149.74	0.54
	40	-20.84		

7

8

9 References

- 10 Abdelhafez, A.A., Li, J., 2016. Removal of Pb(II) from aqueous solution by using biochars
11 derived from sugar cane bagasse and orange peel. *J. Taiwan Inst. Chem. Eng.* 61, 367-375.
- 12 Anwar, J., Shafique, U., Waheed-uz-Zaman, Salman, M., Dar, A., Anwar, S., 2010. Removal of
13 Pb(II) and Cd(II) from water by adsorption on peels of banana. *Bioresource Technol.* 101,
14 1752-1755.
- 15 Cao, Y., Xiao, W., Shen, G., Ji, G., Zhang, Y., Gao, C., Han, L., 2019. Carbonization and ball
16 milling on the enhancement of Pb(II) adsorption by wheat straw: Competitive effects of
17 ion exchange and precipitation. *Bioresource Technol.* 273, 70-76.
- 18 Ding, Z., Wan, Y., Hu, X., Wang, S., Zimmerman, A.Z., Gao, B., 2016. Sorption of lead and
19 methylene blue onto hickory biochars from different pyrolysis temperatures: Importance
20 of physicochemical properties. *J. Ind. Eng. Chem.* 37, 261-267.
- 21 Ho, Y.S., Wase, D.A.J., Forster, C.F., 1996. Kinetic studies of competitive heavy metal
22 adsorption by sphagnum moss peat. *Environ. Technol.* 17, 71-77.
- 23 Komnitsas, K., Zaharaki, D., Pyliotis, I., Vamvuka, D., Bartzas, G., 2015. Assessment of
24 pistachio Shell biochar quality and its potential for adsorption of heavy metals. *Waste
25 Biomass Valori.* 6, 805-816.
- 26 Lee, M., Park, J.H., Chung, J.W., 2019. Comparison of the lead and copper adsorption
27 capacities of plant source materials and their biochars. *J. Environ. Manage.* 236, 118-124.
- 28 Li, Q., Zhai, J., Zhang, W., Wang, M., Zhou, J., 2007. Kinetic studies of adsorption of Pb(II),
29 Cr(III) and Cu(II) from aqueous solution by sawdust and modified peanut husk. *J. Hazard.
30 Mater.* 141, 163-167.
- 31 Liu, Z., Zhang, F., 2009. Removal of lead from water using biochars prepared from
32 hydrothermal liquefaction of biomass. *J. Hazard. Mater.* 167, 933-939.
- 33 Ronda, A., Martín-Lara, M., Dionisio, E., Blázquez, G., Calero, M., 2013. Effect of lead in
34 biosorption of copper by almond shell. *J. Taiwan Inst. Chem. Eng.* 44, 466-473.
- 35 Tan, G., Yuan, H., Liu, Y., Xiao, D., 2010. Removal of lead from aqueous solution with native
36 and chemically modified corncobs. *J. Hazard. Mater.* 174, 740-745.
- 37 Taşar, Ş., Kaya, F., Özer, A., 2014. Biosorption of lead(II) ions from aqueous solution by peanut

38 shells: Equilibrium, thermodynamic and kinetic studies. J. Environ. Chem. Eng. 2, 1018-
39 1026.

40 Wang, C., Wang, H., Cao, Y., 2018. Pb(II) sorption by biochar derived from *Cinnamomum*
41 *camphora* and its improvement with ultrasound-assisted alkali activation. Colloid. Surface.
42 A 556, 177-184.